nature materials

ARTICLES

PUBLISHED ONLINE: 26 OCTOBER 2014 | DOI: 10.1038/NMAT4119

Ferroelectric polarization reversal via successive ferroelastic transitions

Ruijuan Xu[1], Shi Liu[2], Ilya Grinberg[2], J. Karthik[1], Anoop R. Damodaran[1], Andrew M. Rappe[2] and Lane W. Martin[1,3]*

Switchable polarization makes ferroelectrics a critical component in memories, actuators and electro-optic devices, and potential candidates for nanoelectronics. Although many studies of ferroelectric switching have been undertaken, much remains to be understood about switching in complex domain structures and in devices. In this work, a combination of thin-film epitaxy, macro- and nanoscale property and switching characterization, and molecular dynamics simulations are used to elucidate the nature of switching in $PbZr_{0.2}Ti_{0.8}O_3$ thin films. Differences are demonstrated between (001)-/(101)- and (111)-oriented films, with the latter exhibiting complex, nanotwinned ferroelectric domain structures with high densities of 90° domain walls and considerably broadened switching characteristics. Molecular dynamics simulations predict both 180° (for (001)-/(101)-oriented films) and 90° multi-step switching (for (111)-oriented films) and these processes are subsequently observed in stroboscopic piezoresponse force microscopy. These results have implications for our understanding of ferroelectric switching and offer opportunities to change domain reversal speed.

Ferroelectric materials are increasingly being considered as critical components in next-generation logic[1], non-volatile memories[2], actuators and sensors[3], and electro-optic elements for waveguide devices[4]. Such applications require a deep understanding of the susceptibilities (especially to electric fields) and routes to control and manipulate the order parameters in these materials. Recent advances in thin-film synthesis have enabled the manipulation of structure and properties of ferroelectric thin films[5,6]. For example, in the tetragonal ferroelectric $PbZr_{0.2}Ti_{0.8}O_3$ both the domain structure[7,8] and properties (that is, dielectric[9–11], piezoelectric[10,12] and pyroelectric[13,14]) can be widely tuned by varying epitaxial strain, film thickness, electrical boundary conditions and other parameters. So far, the majority of work on such films has focused on (001)-oriented heterostructures, where the possible domain structures have been theoretically predicted[14,15] and observed[14,16]. How these domain structures evolve in other film orientations, however, has not been widely probed[17–19]. Studies of single-crystal ferroelectrics, however, where it is possible to apply the stimulus field along different crystallographic directions, have demonstrated that a poling field that is not purely along the bulk polarization direction produces increased domain wall density and enhanced dielectric[20] and piezoelectric[21] responses. Very few studies on thin-film samples have been completed.

Breakthrough applications of these materials require knowledge of both the static structure and the dynamics of field-dependent responses. Real-time studies of polarization dynamics, including (for example) X-ray scattering[22–24], piezoresponse force microscopy (PFM; refs 25,26), and transmission electron microscopy[27–29] have shed new light on switching processes. Despite these advances, it remains difficult to explore some aspects of switching that take place on very short timescales. Advances in molecular dynamics (MD) simulations now provide an unprecedented look at the dynamics of complex nanoscale events[30], and interatomic potentials derived from *ab initio* calculations can be applied to study finite-temperature properties[31–33] in a variety of environments[34,35]. These studies provide insight into the coupling of polarization, strain, electric field, stress, temperature and local structure; however, there are still very few MD simulations of domain wall motion[30] and domain nucleation and growth rates[36], and the dynamics of 90° domain walls has not been investigated previously.

In this work, we develop a comprehensive picture of the interrelationships between thin-film epitaxy, nanoscale domain structures and electric field switching in $PbZr_{0.2}Ti_{0.8}O_3$. Clear differences are demonstrated between (001)-/(101)- and (111)-oriented films, with the latter exhibiting complex, nanotwinned ferroelectric domain structures with high densities of 90° domain walls, considerably broadened ferroelectric switching characteristics, and lower threshold fields for the onset of nonlinearity in Rayleigh studies. MD simulations reveal the presence of both 180° switching and multi-step 90° switching domain reversal processes. Subsequent stroboscopic PFM studies confirm the presence of intermediate, 90° switching events in (111)-oriented films and 180° switching events in (001)- and (101)-oriented films. The varying effects of domain sizes (or volume fractions) and electric field on the different film orientations give rise to the difference in switching mechanism. These results have implications for our fundamental understanding of ferroelectric switching and provide avenues to accelerate domain reversal in these materials for next-generation applications.

We focus on 150 nm $PbZr_{0.2}Ti_{0.8}O_3$/10 nm $SrRuO_3$ or $La_{0.7}Sr_{0.3}MnO_3$/$SrTiO_3$(001), (110) and (111) heterostructures grown via pulsed-laser deposition (see Methods for details). X-ray diffraction studies show that the films are epitaxial and single-phase (Supplementary Fig. 1). The ferroelectric domain structure was probed using PFM. Throughout the remainder of the discussion, we will use the following terminology to describe the polarization

[1]Department of Materials Science and Engineering, University of California, Berkeley, California 94720, USA. [2]The Makineni Theoretical Laboratories, Department of Chemistry, University of Pennsylvania, Philadelphia, Pennsylvania 19104-6323, USA. [3]Materials Science Division, Lawrence Berkeley National Laboratory, Berkeley, California 94720, USA. *e-mail: lwmartin@berkeley.edu

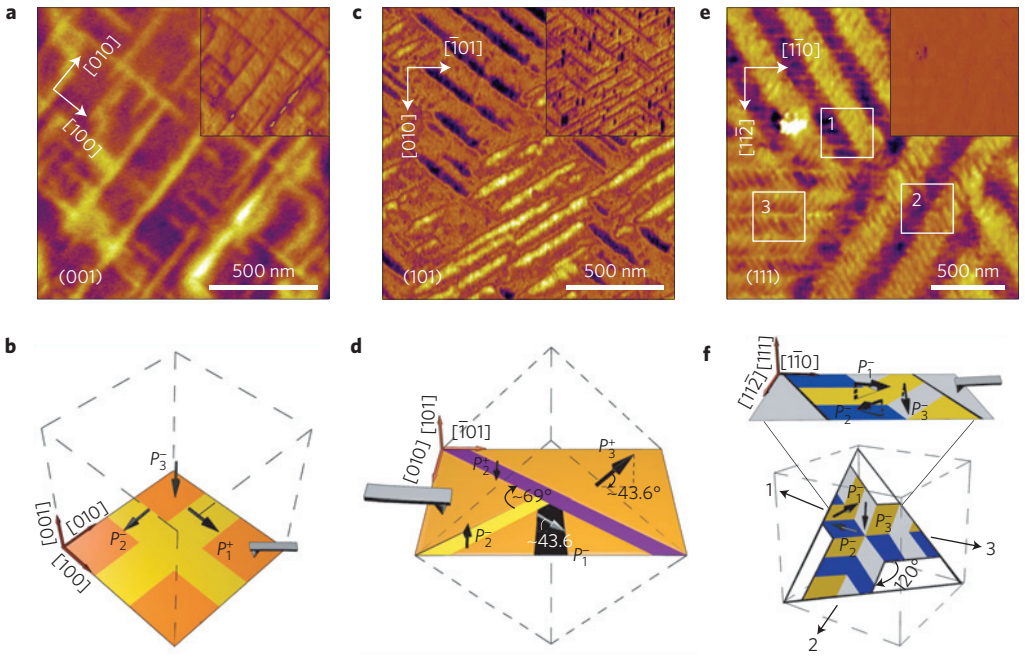

Figure 1 | PFM studies of $PbZr_{0.2}Ti_{0.8}O_3$ films. a–f, Lateral ($A\cos\theta$, combining phase θ and amplitude A) and vertical ($A\cos\theta$, inset) PFM images and schematic illustrations of the domain structures are provided for (001)-oriented heterostructures with majority P_3^- (orange) and minority P_1^+ and P_2^- domains (yellow) (**a**,**b**); (101)-oriented heterostructures with majority P_3^+ (with the polarization oriented at approximately 43.6° from the plane of the film, orange) and minority, stripe-like P_2^+ and P_2^- domains (in-plane polarized, purple) and small fractions of P_1^- domains (with the polarization oriented at approximately 43.6° from the plane of the film, black) (**c**,**d**); (111)-oriented heterostructures with complex nanotwinned domain structures wherein there are three degenerate polarization variants P_1^-, P_2^- and P_3^- oriented at an angle of approximately 33.9° from the plane of the film (represented by yellow, blue and grey, respectively), which are tiled to produce three degenerate domain bands separated by 120°, as labelled in the squares 1, 2 and 3 (**e**,**f**).

variants in the samples: for tetragonal $PbZr_{0.2}Ti_{0.8}O_3$, domains with polarization along the positive and negative [100], [010] and [001] axes will be referred to as $P_1^{+/-}$, $P_2^{+/-}$ and $P_3^{+/-}$, respectively. In (001)-oriented heterostructures, a typical polydomain structure with majority P_3^- domains and minority P_1^+ and P_2^- domains is observed (Fig. 1a,b). In (101)-oriented heterostructures, three different domain types are found (Fig. 1c,d), with majority P_3^+ domains (in which the polarization is oriented at an angle of approximately 43.6° from the plane of the film) and the remainder is primarily composed of in-plane polarized stripe-like P_2^+ and P_2^- domains and small fractions of P_1^- domains (also oriented approximately 43.6° from the plane of the film). The as-grown domain structure of the (001)- and (101)-oriented films, as probed by PFM studies which enable exact determination of the polarization directions, represents the equilibrium domain structure predicted for these film orientations[37,38] and does not change with electric field cycling (Supplementary Fig. 2a,b).

Analysis of the (111)-oriented heterostructures reveals a markedly different picture. The as-grown domain structure has a complex, metastable nanoscale domain pattern (Supplementary Fig. 2c,d). A domain structure consistent with that predicted for the equilibrium domain structure is obtained after a series of ±6 V d.c. voltages was applied to the PFM tip to switch a 1.5 μm × 1.5 μm region of the film a total of two to six times. The domain pattern consists of a high density of nanotwinned domains (Fig. 1e). The observed domain structure is the result of the tiling of three types of domain bands, separated by 120° (noted as areas 1, 2 and 3, Fig. 1e) with average domain bandwidths of ≈300 nm. Within each domain band, the domain structure consists of a mixture of all three degenerate polarization variants (P_1^-, P_2^- and P_3^-, each possessing a polarization direction that is oriented at an angle of approximately 33.9° from the plane of the film) distributed into two subbands, with each subband composed of only two of the polarization variants. The average domain size within the domain subbands is approximately 40 nm. The geometry of such domain structures is shown in a schematic illustration (Fig. 1f). Prior theoretical treatments have predicted such equilibrium domain structures[39].

Having established the difference in domain structures for the various heterostructure orientations, we probed their dielectric and ferroelectric properties using symmetric metal-oxide capacitor structures[40] and MD simulations (see Methods for details). All heterostructures, regardless of orientation, were found to exhibit symmetric, well-saturated polarization–electric field hysteresis loops (Fig. 2a), which are maintained down to at least 1 Hz (Supplementary Fig. 3). As expected, the saturation polarization scales with the film orientation, with (001)- and (111)-oriented films having the largest and smallest values, respectively. Furthermore, although all films possess high remnant polarization, the (001)- and (101)-oriented films show nearly square hysteresis loops with sharp electric field switching, whereas (111)-oriented films exhibit more slanted hysteresis loops regardless of frequency, indicative of switching at a broader range of fields (Supplementary Fig. 4).

The dielectric permittivity was then measured as a function of increasing a.c. electric field excitation. As we are focused here on switching behaviour, we have extended this analysis to larger fields than are typically applied in Rayleigh studies (details of which are provided in the Supplementary Fig. 5; ref. 41). These studies reveal that (111)-oriented heterostructures exhibit a lower threshold field (8.2 kV cm^{-1}) for the onset of nonlinearity (or polarization switching) than (001)- and (101)-oriented films (46.3 kV cm^{-1} and 22.5 kV cm^{-1}, respectively) (Fig. 2b). Furthermore, the field dependence of the dielectric response of the (111)-oriented film shows a gradual increase (and, therefore, ferroelectric switching) over a much larger range of fields, relative to the (001)- and (101)-oriented films, consistent with the polarization–electric field hysteresis loops (Fig. 2a).

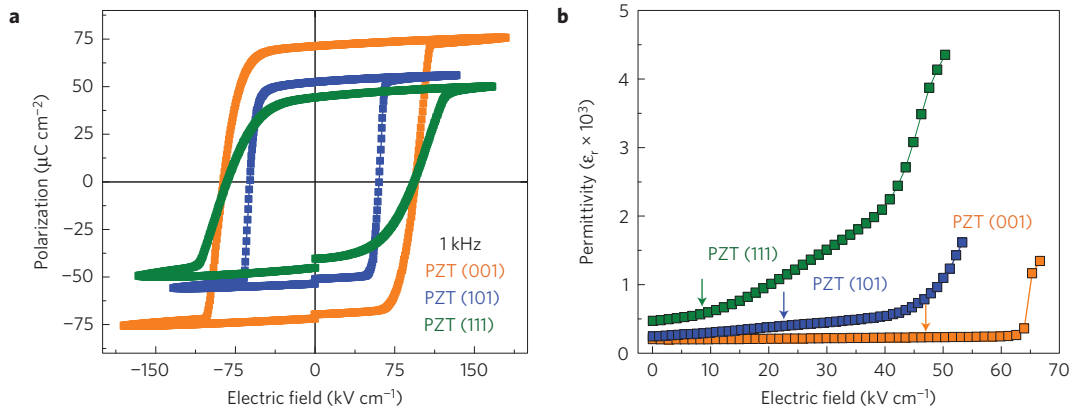

Figure 2 | Electrical characterization of $PbZr_{0.2}Ti_{0.8}O_3$ films. a,**b**, Polarization–electric field hysteresis loops (**a**) and permittivity as a function of a.c. electric field (**b**) measured at 1 kHz for (001)-, (101)- and (111)-oriented $PbZr_{0.2}Ti_{0.8}O_3$ (PZT) thin films. The arrows demarcate the location of the onset of nonlinearity from the Rayleigh studies.

To understand what gives rise to these different electric field responses, we used MD simulations to examine the evolution of domain switching under differently oriented electric fields. We studied the evolution of domain structures resembling those experimentally observed in (001)-, (101)- and (111)-oriented films possessing 90° domain walls under electric fields applied along the film normal directions $[00\bar{1}]$, $[\bar{1}0\bar{1}]$ (Fig. 3a) and $[\bar{1}\bar{1}\bar{1}]$ (Fig. 3b), respectively. The volume fraction of the minority domain used in the simulations is based on experimental observations. The MD simulations provide a time-resolved view of the evolution of the domain structure, including specific polarization variants (Supplementary Fig. 6).

For brevity, we discuss here only the detailed MD studies of (101)-oriented films, but detailed studies of (001)-oriented films, which show similar results, are also provided (Supplementary Fig. 7). In the case of (101)-oriented films, in the initial state (0 ps) we simulate a domain configuration with 20% minority P_2^+ domains (green, Fig. 3a) and 80% majority P_1^+ domains (red, Fig. 3a) with the electric field applied along $[\bar{1}0\bar{1}]$ (yellow arrow, Fig. 3a). This results in a series of complicated changes (Fig. 3a). At 3 ps, we observe that the volume fraction of P_2^+ domains increases as they widen via changes of the type $P_1^+ \rightarrow P_2^+$ at the domain boundary owing to the $[\bar{1}00]$-component of the electric field. Also, a significant number of P_1^+ dipoles close to domain boundaries are switched by 180° to P_1^- dipoles (cyan). Further application of the electric field facilitates the growth of the P_1^- domains via the 180° switching process of $P_1^+ \rightarrow P_1^-$ (see the 5 ps and 7 ps images, Fig. 3a). At 10 ps, the whole supercell reaches a nearly single-domain state. Subsequent relaxation of the structure (after the field is turned off) for another 30 ps results in the re-emergence of domain structures similar to those in the initial state (albeit poled in the opposite direction) due to strain accommodation. The lateral shift of the domain boundary is probably due to the application of the large electric field to achieve picosecond switching in the MD simulations.

In the case of (111)-oriented films, in the initial state (0 ps) we simulate a domain configuration with 50% P_1^+ domains (red, Fig. 3b) and 50% P_2^+ domains (green, Fig. 3b) with the electric field applied along $[\bar{1}\bar{1}\bar{1}]$ (yellow arrow, Fig. 3b). This process results in a fundamentally different domain switching evolution (Fig. 3b). First, we observe that there is no significant domain wall motion. Although decidedly different from the behaviour in (101)-oriented films, this is expected as all polarization directions are energetically equivalent with respect to the applied field. Also, at 5 ps, we see new domains perpendicular to their parent domains appear via two types of 90° switching processes: $P_1^+ \rightarrow P_2^-$ and $P_2^+ \rightarrow P_1^-$, respectively. By 8 ps, the new domains spread quickly across their parent domains and dipole frustration at domain boundaries, leading to transient charged domain walls, is also observed (Supplementary Fig. 8; ref. 42). This switching process continues, until the final configuration of P_1^- and P_2^- domains is achieved by 10 ps. The strain-driven structural relaxation for another 10 ps in the absence of electric field leads to a slight change in the positions of domain walls, but overall the re-emergence of domain structures similar to those in the initial state (albeit poled in the opposite direction).

What these MD simulations reveal is that, if one considers only the starting and final states, the domain structures could potentially lead one to assume only 180° switching has taken place on the macroscale. These time-dependent models, however, reveal a more nuanced evolution, with clear differences between (001)-/(101)- and (111)-oriented films, with the latter revealing a multi-step, 90° switching domain reversal process. To further explore these proposed switching pathways and their implications for material properties, we completed local-scale PFM switching studies where a time series of images was produced while incrementally increasing the applied tip bias. Focusing first on switching in the (001)- and (101)-oriented films, similarly abrupt switching processes occurring in a narrow field range have been observed, consistent with the macroscale property studies. For brevity, we discuss here only the detailed switching studies of (101)-oriented films (Fig. 4), but detailed studies of (001)-oriented films are provided (Supplementary Fig. 9). The (101)-oriented films show no obvious contrast change in either the lateral or vertical PFM images (Fig. 4a,b) when applying biases from 0.0 to 3.0 V to locally switch a 1 μm × 1 μm square region in the centre of the scanned area. A schematic of this domain structure before switching is provided (Fig. 4c). On increasing the applied tip bias further, to 3.5 V, domains in the film start to switch, resulting in a contrast change in both the lateral and vertical PFM images (Fig. 4d). Further increasing the bias to 4.0 V results in complete switching of the central square region (Fig. 4e). Based on the PFM images, the final switched domain structure is interpreted such that both domains initially possessing polarization P_3^+ (orange regions, Fig. 4c) and in-plane-oriented stripe domains P_2^- and P_2^+ (black and grey regions, Fig. 4c) are switched by 180° (Fig. 4f). These observations are consistent with the abrupt switching that occurs in a narrow field range in the polarization hysteresis loops and with the abrupt increase of dielectric response in the Rayleigh analysis. These results indicate that 180° switching reversal occurs in (101)-oriented films, in agreement with MD predictions.

Similar studies of (111)-oriented films, however, reveal decidedly different responses, with a complex evolution of domain structures involving four characteristic steps in the switching (Fig. 5a–d).

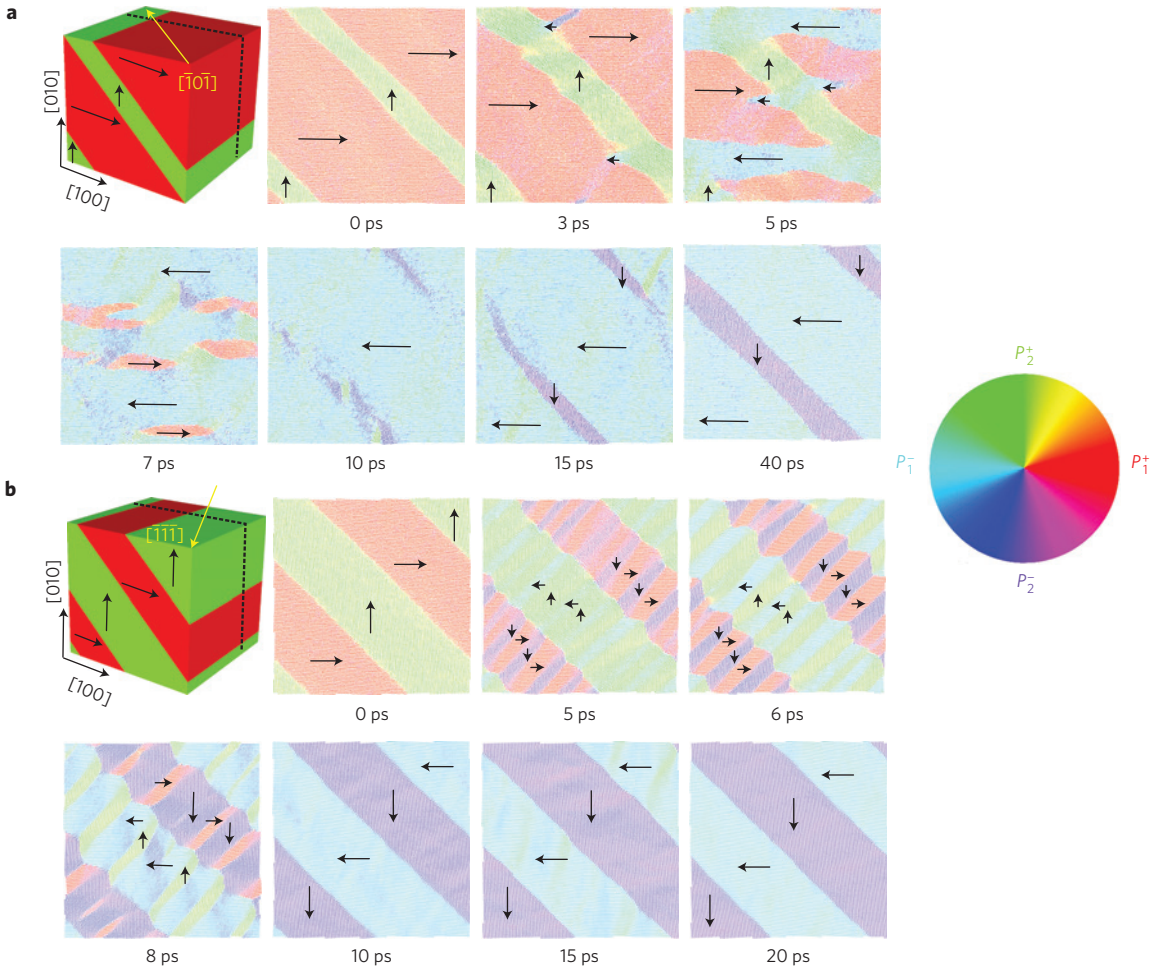

Figure 3 | MD simulations of switching in ferroelectrics with 90° domain walls. For all simulations, the electric field is turned on at 0 ps and off at 10 ps and the domain structures are allowed to relax at zero applied field from that point. **a**, Domain evolution in (101)-oriented films possessing 20% of minority P_2^+ domains (green) and 80% of majority P_1^+ domains (red) under an applied field along [$\bar{1}0\bar{1}$] (yellow arrow). Direct 180° polarization reversal is observed ($P_2^+ \rightarrow P_2^-$ and $P_1^+ \rightarrow P_1^-$). **b**, Domain evolution in (111)-oriented films possessing 50% P_2^+ domains (green) and 50% P_1^+ domains (red) under an applied field along the [$\bar{1}\bar{1}\bar{1}$] (yellow arrow). Only 90° polarization switching events ($P_2^+ \rightarrow P_1^-$ and $P_1^+ \rightarrow P_2^-$) are observed. The local polarization within each unit cell is represented by an arrow coloured according to the polarization wheel.

Detailed static domain structure characterization of the (111)-oriented films has been discussed above, and here we focus on an area possessing fully down-poled nanotwinned domain bands of a single type for simplicity (Fig. 5a). When applying a tip bias of −2.5 V to locally switch a 1 μm × 1 μm square region, only a small fraction of the domains switch (inset, Fig. 5b). Examination of the lateral PFM contrast reveals that the orientation of the long axes of the domains that were switched rotates by 90° in the plane of the film, resulting in a new domain configuration with a characteristic angle of 60° between the domain subbands (Fig. 5b). On further increasing the bias to −3.5 V, the majority of the square region subjected to the bias has been switched to the out-of-plane direction (inset, Fig. 5c), with the contrast changing accordingly in the lateral PFM images to reveal a characteristic angle of 60° between all domain subbands in the switched region (Fig. 5c). The domain structure does not exhibit further evolution until the applied tip bias exceeds −6 V. At this point, all domains in the square region subjected to the bias have become fully up-poled (inset, Fig. 5d). The nanotwinned domain pattern is observed to return to the initial orientation and re-establishes the characteristic angle of 120° between the long axes of the domains (Fig. 5d). Although a similar nanotwinned domain structure has been achieved, the in-plane contrast in the nanotwinned array has changed from that of the initial state (that is, subbands with dark PFM contrast become light and vice versa, Fig. 5d) suggesting that full switching is accompanied by an orientation change of the in-plane component of polarization.

This multi-step switching process is intriguing, and here we systematically analyse it. We provide schematic illustrations of the geometry of the sample, including the crystallographic axes (Fig. 5e), the six possible polarization variants (Fig. 5f), and the twelve possible (six distinct) 90° domain boundaries (that is, those between P_1^+-P_2^+ (P_1^--P_2^-), P_1^+-P_3^+ (P_1^--P_3^-), P_2^+-P_3^+ (P_2^--P_3^-), P_1^+-P_2^- (P_1^--P_2^+), P_1^+-P_3^- (P_1^--P_3^+), P_2^+-P_3^- (P_2^--P_3^+); each given a unique colour in the figure) (Fig. 5g) projected on the (111) of the PFM image. Further details of the geometry of the domain boundaries are provided (Supplementary Fig. 10). To aid the discussion, we provide schematic illustrations of the domain structures (Fig. 5h–o) in each distinct domain subband type for the four PFM images (Fig. 5a–d). Three different colours (orange, blue and grey) are used to represent the three different polarization variants, with solid and dashed lines corresponding to down- and up-poled versions, respectively. In the initial state (Fig. 5a), all domains are down-poled, and the dark (Fig. 5h) and light (Fig. 5i) domain subbands consist of alternating P_1^-/P_2^- and P_1^-/P_3^- domains, respectively. On application of the −2.5 V applied bias (Fig. 5b), the orientations of the domain boundaries in both the dark (Fig. 5j) and light (Fig. 5k)

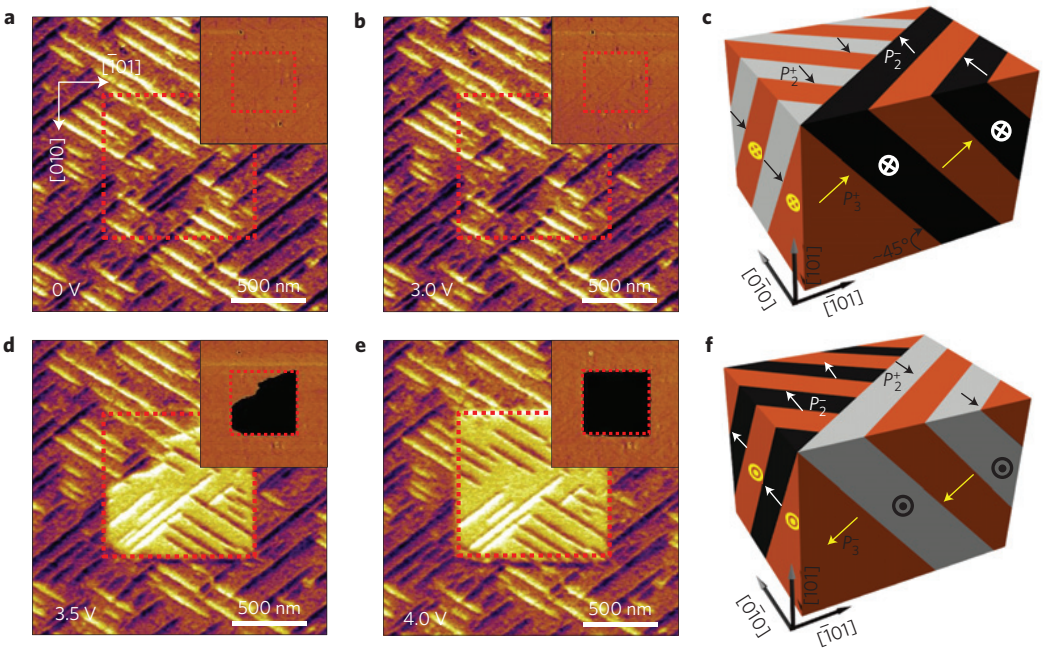

Figure 4 | PFM switching studies of $PbZr_{0.2}Ti_{0.8}O_3$ (101) thin films. a,**b**, Lateral ($A\cos\theta$, combining phase θ and amplitude A) and vertical (phase θ, inset) PFM images of field-dependent domain structure evolution in (101)-oriented $PbZr_{0.2}Ti_{0.8}O_3$ in the as-grown state (**a**) and after applying a tip bias of 3.0 V in the central square region (**b**). **c**, Schematic illustration of the observed, unswitched domain structure with the majority P_3^+ domains (orange, oriented at an angle of 43.6° from the plane of the film) and stripe-like P_2^- (black) and P_2^+ (grey) domains (in-plane polarized). **d**,**e**, On increasing the applied tip bias to 3.5 V (**d**) and 4.0 V (**e**), abrupt switching is observed. **f**, Schematic illustration of the switched domain structure in **d** and **e** with the majority P_3^- (orange), P_2^- (black), and P_2^+ (grey) domains after the 180° switching.

domain subbands are found to rotate by 90° in the plane of the film. Such a change in the domain boundary orientation can be achieved only by a complex switching process which includes three different switching events (Fig. 5j), including 90° switching that maintains the vertical component of the polarization ($P_1^- \rightarrow P_2^-$, area 1), 180° switching ($P_1^- \rightarrow P_1^+$, area 2), and 90° switching that changes the vertical component of the polarization ($P_2^- \rightarrow P_1^+$, area 3), as well as regions that experience no switching ($P_2^- \rightarrow P_2^-$, area 4). Similar complex switching occurs in the light domain subbands as well (Fig. 5k). On further increasing the bias to −3.5 V (Fig. 5c), the orientation of the domain boundaries remains the same, but all domains are now up-poled (Fig. 5l,m), with a change of the in-plane contrast from light to dark (and vice versa) for the different domain subband types. This switching process (Fig. 5l) includes 90° switching that maintains the vertical component of the polarization ($P_1^+ \rightarrow P_2^+$) and 90° switching that changes it ($P_2^- \rightarrow P_1^+$). Similar 90° switching events occur in the other domain subbands (Fig. 5m). Based on the PFM analysis, this up-poled domain structure should probably possess charged domain walls; however, it is not changed until the applied bias is further increased to −6 V (Fig. 5d). At this point, the domain boundaries are again rotated in the plane of the film by 90° and the domain structure is returned to a configuration consistent with the initial state (Fig. 5n,o), but with a change of the in-plane contrast in the PFM from light to dark (and vice versa) for the different domain subband types. Again, the domain walls in the final state are uncharged. This process is again accomplished by two types of 90° switching events that maintain the vertical component of the polarization ($P_1^+ \rightarrow P_2^+$ and $P_2^+ \rightarrow P_1^+$, Fig. 5n). Again, similar 90° switching events are observed for both domain subband types (Fig. 5o). In the end, regardless of how the switching is probed and acknowledging potential differences in the fine-scale nature of excitation and final domain structure produced by the different methodologies, the mechanisms underlying the switching events are innate to the materials. Thus, the combination of macroscopic capacitor, scanning-probe and MD studies provides a detailed, multiple length and timescale look at the switching in these materials. From these studies, we observe that (001)-/(101)-oriented films switch via 180° switching processes whereas (111)-oriented films undergo domain reorientation via 90° switching processes.

Although the nucleation-and-growth process for 180° switching events is fairly well understood, little evidence for 90°-switching-mediated domain reversal has been presented. It has been suggested that broadened (or double) current peaks during reverse switching of previously poled $PbZr_{0.415}Ti_{0.585}O_3$ ceramics could be the result of non-180° domain switching due the residual stresses developed during forward poling[43] and that in single crystals of [111]-oriented 95.5% $PbZn_{1/3}Nb_{2/3}O_3$–4.5% $PbTiO_3$, polarization reversal through intermediate polarization rotations of 71° and 109° can occur[44,45]. Despite these observations, the mechanisms underlying such behaviour are not entirely clear[46] and no direct measurements and examples of 90°-switching-mediated domain reversal have been reported in the literature. This is particularly the case for thin films, where there are no reports in this regard. In thin films, the 90° domain switching process, due to the elastic clamping of the substrate, is thought to be so energetically costly that it does not typically occur. Enhanced 90° domain switching can be realized in thin films if the effect of clamping can be compensated by engineering specific film or domain structures such as in patterned ferroelectric layers[47] or through a layered structure where the top layer is anchored on an underlying layer of a secondary ferroelectric phase[48]. Here we have achieved the 90°-switching-mediated domain reversal process in thin films by using (111)-oriented domain structures, where the energetics are such that it permits these events to take place.

The preference for a 90° or 180° switching process in different films is ultimately controlled by the clamping of the ferroelectric film (and the resulting domain size). In both (001)-/(101)-oriented heterostructures, the elastic constraints from the substrate lead

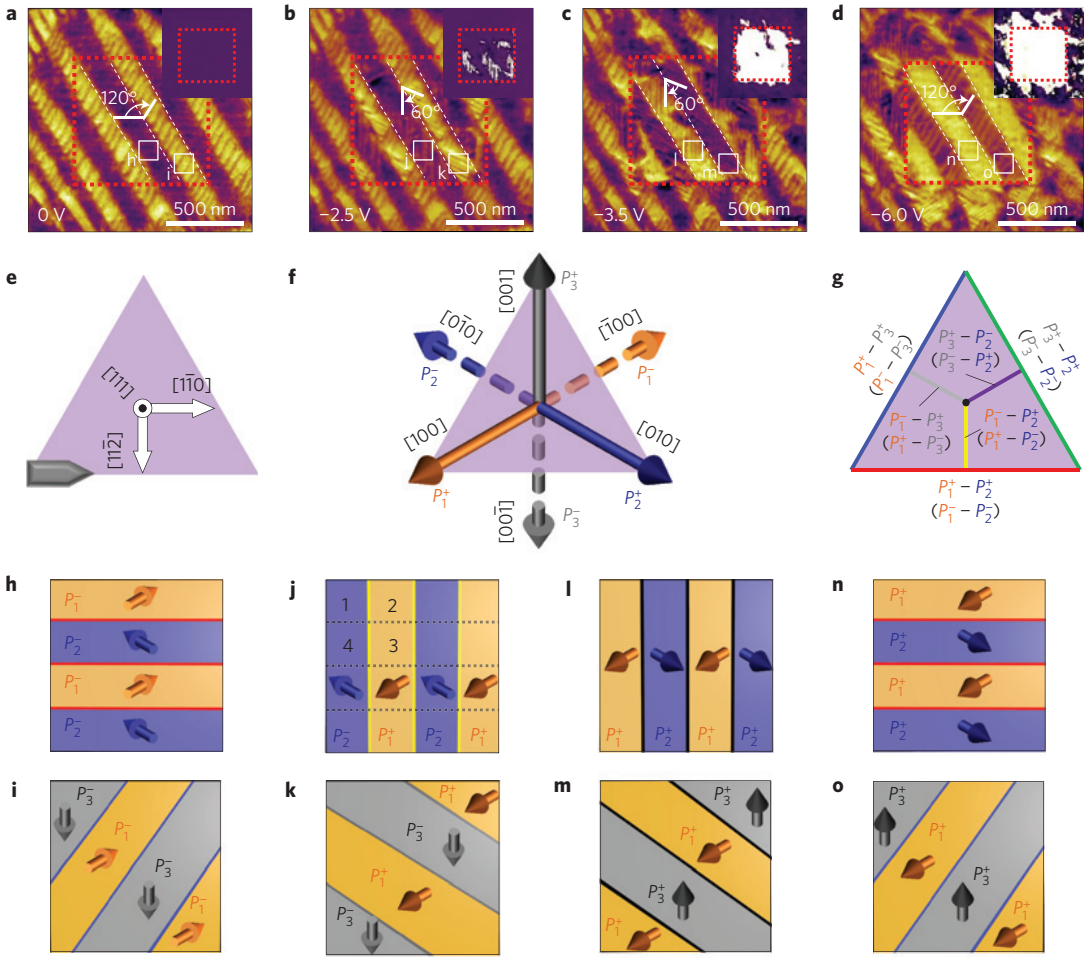

Figure 5 | PFM switching studies of $PbZr_{0.2}Ti_{0.8}O_3$(111) thin films. a–d, Lateral ($A\cos\theta$, combining phase θ and amplitude A) and vertical (phase θ, inset) PFM images of domain structure evolution in (111)-oriented $PbZr_{0.2}Ti_{0.8}O_3$ in the initial down-poled state (**a**), after applying a tip bias of −2.5 V (partial switching; **b**), −3.5 V (complete out-of-plane, incomplete in-plane switching; **c**) and −6.0 V (complete out-of-plane and in-plane switching; **d**). **e–g**, Schematic illustrations of the projection of the crystallographic axes (**e**), six possible polarization variants (solid and dashed pointing out and into the film plane, respectively) (**f**) and six possible distinct 90° domain boundaries (**g**) (each given a unique colour that is carried throughout the remaining panels). **h–o**, Further illustrations of the switching process for dark and light domain bands, respectively, for the initial state (**h**,**i**), a majority down-poled intermediate state (**j**,**k**), an up-poled intermediate state (**l**,**m**) and the final state (**n**,**o**).

to large differences in the fraction of in-plane and out-of-plane polarized domains (in particular, minimizing the fraction of in-plane polarized domains). Although 90° domain walls have lower domain wall energy than 180° domain walls[49], 90° ferroelastic switching in thin films is generally unfavourable in comparison with 180° ferroelectric switching (as we observed for (001)-/(101)-oriented films in our simulations) under moderate electric fields because of the large energy penalty associated with the change of volume fractions of in-plane and out-of-plane polarized domains that must occur to accommodate such switching events[50]. Said another way, the free-energy change (Δf) for a ferroelastic 90° switching event is dominated by contributions from the stress (σ^2) and the stress–polarization coupling (σP^2) terms. These energy terms are high in the (001)-/(101)-oriented films owing to the elastic constraints of the substrate and the drastically different stress states for an in-plane or out-of-plane polarized domain. On the other hand, the (111)-oriented films possess three energetically degenerate polarization variants (in a fully poled state), all possessing in-plane and out-of-plane polarization components that are the same and, in effect, renders the elastic energy costs associated with a ferroelastic 90° switching event greatly reduced. Furthermore, our MD simulations reveal that coordinated 90° switching events (that is, $P_1^+ \rightarrow P_2^-$ and $P_2^+ \rightarrow P_1^-$) occur in essentially equal proportions across the entire domain width to accommodate (and maintain) both the elastic and electrostatic energy state of the system. As a result, the coordinated, multi-step 90° switching process will not incur a large elastic energy cost, in agreement with the arguments above. Ultimately the preference of 90° switching over 180° switching in the (111)-oriented films is due to the lower kinetic barrier for 90° polarization rotation indicated by the lower energy of the 90° domain wall compared to that of the 180° domain wall.

The observation of such 90°-switching-mediated domain reversal, in turn, has important implications for our overall understanding of ferroelectric materials and their utilization in devices. First, the presence of active intermediate switching states can be correlated to the differences observed in the dielectric and ferroelectric response of the various orientations of films. Although all films possess high remnant polarization, the (001)-/(101)-oriented films show nearly square hysteresis loops, with sharp electric field switching (consistent with 180° switching events), whereas (111)-oriented films exhibit more slanted hysteresis loops,

with larger coercive fields, indicative of switching at a broader range of fields and a multi-step switching process. Furthermore, it is likely that the availability of low-field intermediate switching can account for the observation of lower threshold fields for the nucleation of switching events in the Rayleigh studies of the (111)-oriented films. The domain reversal process is significantly impacted by changing the orientation of the epitaxial film and by allowing all possible switching types to be active in the material. Ultimately, if we can create pathways similar to those demonstrated in the stroboscopic PFM studies by which to deterministically stabilize or incrementally step the switched polarization from one state, through a number of intermediate states, before reaching the oppositely poled state, the possibility for creating new modalities of low-power, multi-state memory or logic can be imagined. At the same time, if we can determine ways to promote the 90°-switching-mediated domain reversal process, this could further accelerate the domain reversal and reduce the timescale of ferroelectrics, thereby increasing the potential for their use in advanced nanoelectronics.

In conclusion, we have observed both 180° and multi-step 90° switching domain reversal processes in $PbZr_{0.2}Ti_{0.8}O_3$ thin films. Using a combination of epitaxial thin-film growth, macro- and nanoscale characterization and MD simulations, we have been able to manipulate the domain structure through the control of film orientations and explore the coupling between the domain structures and properties. Specifically, stark differences between (001)-/(101)- and (111)-oriented films were observed, with the latter exhibiting complex, nanotwinned ferroelectric domain structures with high densities of 90° domain walls, considerably broadened ferroelectric switching characteristics, and lower threshold fields for the onset of nonlinearity during Rayleigh studies. Subsequent MD simulations and PFM studies reveal both types of switching mechanisms are possible, but that the switching process that ultimately occurs is determined by a combination of factors, including domain wall energy, elastic strain and domain size. These observations provide insight into a previously unexplored aspect of ferroelectric switching and highlight the complexity of these materials. Such studies are crucial for developing precise control of nanoscale ferroelectric materials and can potentially lead to interesting multi-state devices and accelerated switching in ferroelectrics.

Methods

Epitaxial thin-film growth. The growth of $PbZr_{0.2}Ti_{0.8}O_3$ was carried out at an oxygen pressure of 200 mtorr at 635° C with a laser fluence of 0.9–1.0 J cm^{-2} and a laser repetition rate of 3 Hz. The growth of $SrRuO_3$ and $La_{0.7}Sr_{0.3}MnO_3$ was accomplished at oxygen pressures of 100 mtorr and 200 mtorr, respectively, at 645 °C with laser repetition rates of 12 Hz and 3 Hz, respectively. After the growth, the samples were cooled at 5 °C min^{-1} in an oxygen pressure of 760 torr. We note that the crystal and domain structure and properties of $PbZr_{0.2}Ti_{0.8}O_3$ films grown on either $SrRuO_3$ or $La_{0.7}Sr_{0.3}MnO_3$ bottom electrodes are essentially the same; thus, the data from heterostructures with both electrode layers are used interchangeably.

Crystal and domain structure characterization. X-ray θ–2θ scans were obtained by high-resolution X-ray diffraction (XPert MRD Pro equipped with a PIXcel detector, Panalytical). The PFM studies were carried out on a Cypher (Asylum Research) AFM using Ir/Pt-coated conductive tips (Nanosensor, PPP-NCLPt, force constant ≈48 N m^{-1}). The detailed polarization maps were generated under the single frequency vector PFM mode, which enables the simultaneous imaging of the phase (θ) and amplitude (A) from both the lateral and vertical piezoresponse signal. To elucidate the PFM contrast, the PFM signals were processed in the form of a combination ($A\cos\theta$) of phase and amplitude.

Electrical measurements. All the electrical measurements were performed on capacitor structures of $PbZr_{0.2}Ti_{0.8}O_3$ films with symmetric electrodes of $SrRuO_3$ or $La_{0.7}Sr_{0.3}MnO_3$. The patterned circular top electrodes were fabricated by means of a MgO hard mask technique[40] and the measurement was conducted on capacitors with the top electrode diameter ranging from 25 μm to 200 μm. The polarization–electric field hysteresis loops were measured using a Precision Multiferroic Tester (Radiant Technologies). The room-temperature permittivity was measured using an E4980A LCR meter (Agilent Technologies). All samples were pre-poled before the dielectric measurement. During the measurement, the bottom electrode was driven by an increasing a.c. electric field at 1 kHz.

Molecular dynamics simulations. Domain reversal in $PbTiO_3$ under applied electric fields was modelled with molecular dynamics. We use a bulk, stoichiometric $PbTiO_3$ supercell. We carry out molecular dynamics simulations under periodic boundary conditions with fixed dimensions. The supercell lengths and angles are slightly adjusted based on the volume fraction (γ) of the minority domain (green domains shown in Fig. 3) to simulate the mechanical clamping effect consistent with the epitaxial thin film in experiments. Although a thin film clamped in the two in-plane directions in principle can be modelled with a slab geometry, applying such a model with mixed elastic boundary conditions is technically difficult in MD simulations and will also complicate the understanding of the switching mechanism after introducing surface and size (thickness) effects. Our bulk model corresponds to a sample clamped in all three Cartesian directions. This was done by design to enable us to focus on the intrinsic response of the material, allowing us to separate the switching behaviour due to domain structure and strain as opposed to that influenced by the surface and other extrinsic effects. The simulations are performed with a bond-valence-based interatomic potential with a timestep of 1.0 fs at 200 K. The domain structure is modelled with a $120a_1 \times 120a_2 \times 4a_3$ supercell, where a_1, a_2 and a_3 are the averaged lattice constants. See details in Supplementary Information for equations calculating supercell dimensions. The electric field is applied for 10 ps along $[\bar{1}0\bar{1}]$ to the supercell with $\gamma = 0.2$ and along $[\bar{1}\bar{1}\bar{1}]$ to the supercell with $\gamma = 0.5$, to resemble the actual field orientations experienced by (101) and (111) thin films of similar volume fractions in experiments. After the field removal, we allow the system to evolve freely with supercell dimensions conserved. As the structure and polarization of $PbZr_{0.2}Ti_{0.8}O_3$ are similar to those of $PbTiO_3$, we expect that the domain switching mechanisms modelled with $PbTiO_3$ are applicable to $PbZr_{0.2}Ti_{0.8}O_3$.

Received 22 October 2013; accepted 23 September 2014; published online 26 October 2014

References

1. Hoffman, J. *et al.* Ferroelectric field effect transistors for memory applications. *Adv. Mater.* **22,** 2957–2961 (2010).
2. Scott, J. F. Applications of modern ferroelectrics. *Science* **315,** 954–959 (2012).
3. Eom, C. B. & Trolier-McKinstry, S. Thin-film piezoelectric MEMS. *MRS Bull.* **37,** 1007–1021 (2012).
4. Wessels, B. W. Ferroelectric epitaxial thin-films for integrated optics. *Annu. Rev. Mater. Res.* **37,** 659–679 (2007).
5. Dawber, M., Rabe, K. M. & Scott, J. F. Physics of thin-film ferroelectric oxides. *Rev. Mod. Phys.* **77,** 1083–1130 (2005).
6. Martin, L. W. & Schlom, D. G. Advanced synthesis techniques and routes to new single-phase multiferroics. *Curr. Opin. Solid State Mater. Sci.* **16,** 199–215 (2012).
7. Nagarajan, V. *et al.* Thickness dependence of structural and electrical properties in epitaxial lead zirconate titanate films. *J. Appl. Phys.* **86,** 595–602 (1999).
8. Li, Y. L., Hu, S. Y., Liu, Z. K. & Chen, L. Q. Effect of electrical boundary conditions on ferroelectric domain structures in thin films. *Appl. Phys. Lett.* **81,** 427–429 (2002).
9. Pertsev, N. A., Arlt, G. & Zembilgotov, A. G. Domain-wall and intrinsic contributions to the dielectric response of epitaxial ferroelectric films. *Microelectron. Eng.* **29,** 135–140 (1995).
10. Xu, F. *et al.* Domain wall motion and its contribution to the dielectric and piezoelectric properties of lead zirconate titanate films. *J. Appl. Phys.* **89,** 1336–1348 (2001).
11. Karthik, J., Damodaran, A. R. & Martin, L. W. Effect of 90° domain walls on the low-field permittivity of $PbZr_{0.2}Ti_{0.8}O_3$ thin films. *Phys. Rev. Lett.* **108,** 167601 (2012).
12. Kim, D. J., Maria, J. P., Kingon, A. I. & Streiffer, S. K. Evaluation of intrinsic and extrinsic contributions to the piezoelectric properties of $Pb(Zr_{1-x}Ti_x)O_3$ thin films as a function of composition. *J. Appl. Phys.* **93,** 5568–5575 (2003).
13. Bruchhaus, R., Pitzer, D., Schreiter, M. & Wersing, W. Optimized PZT thin films for pyroelectric IR detector arrays. *J. Electroceram.* **3,** 151–162 (1999).
14. Karthik, J. & Martin, L. W. Pyroelectric properties of polydomain epitaxial $Pb(Zr_{1-x}Ti_x)O_3$ thin films. *Phys. Rev. B* **84,** 024102 (2011).
15. Pertsev, N. A., Kukhar, V. G., Kohlstedt, H. & Waser, R. Phase diagrams and physical properties of single-domain epitaxial $Pb(Zr_{1-x}Ti_x)O_3$ thin films. *Phys. Rev. B* **67,** 054107 (2003).
16. Pertsev, N. A. & Zembilgotov, A. G. Domain populations in epitaxial ferroelectric thin films: Theoretical calculations and comparison with experiment. *J. Appl. Phys.* **80,** 6401–6406 (1996).

17. Saito, K., Kurosawa, T., Akai, T., Oikawa, T. & Funakubo, H. Structural characterization and 90 degrees domain contribution to ferroelectricity of epitaxial $Pb(Zr_{0.35},Ti_{0.65})O_3$ thin films. *J. Appl. Phys.* **93,** 545–550 (2003).
18. Oikawa, T., Aratani, M., Funakubo, H., Saito, K. & Mizuhira, M. Composition and orientation dependence of electrical properties of epitaxial $Pb(Zr_xTi_{1-x})O_3$ thin films grown using metalorganic chemical vapor deposition. *J. Appl. Phys.* **95,** 3111–3115 (2004).
19. Xu, R., Karthik, J., Damodaran, A. R. & Martin, L. W. Stationary domain wall contribution to enhanced ferroelectric susceptibility. *Nature Commun.* **5,** 3120 (2014).
20. Bernal, A., Zhang, S. J. & Bassiri-Gharb, N. Effects of orientation and composition on the extrinsic contributions to the dielectric response of relaxor-ferroelectric single crystals. *Appl. Phys. Lett.* **95,** 142911 (2009).
21. Wada, S., Yako, K., Kakemoto, H., Tsurumi, T. & Kiguchi, T. Enhanced piezoelectric properties of barium titanate single crystals with different engineered-domain sizes. *J. Appl. Phys.* **98,** 014109 (2005).
22. Grigoriev, A. *et al.* Nanosecond domain wall dynamics in ferroelectric $Pb(Zr,Ti)O_3$ thin films. *Phys. Rev. Lett.* **96,** 187601 (2006).
23. Jo, J. Y. *et al.* Nanosecond dynamics of ferroelectric/dielectric superlattices. *Phys. Rev. Lett.* **107,** 055501 (2011).
24. Zubko, P., Stucki, N., Lichtensteiger, C. & Triscone, J. M. X-ray diffraction studies of 180° ferroelectric domains in $PbTiO_3$/$SrTiO_3$ superlattices under an applied electric field. *Phys. Rev. Lett.* **104,** 187601 (2010).
25. Kalinin, S. V. *et al.* Defect-mediated polarization switching in ferroelectrics and related materials: From mesoscopic mechanisms to atomistic control. *Adv. Mater.* **22,** 314–322 (2010).
26. Gruverman, A. *et al.* Direct studies of domain switching dynamics in thin film ferroelectric capacitors. *Appl. Phys. Lett.* **87,** 082902 (2005).
27. Nelson, C. T. *et al.* Domain dynamics during ferroelectric switching. *Science* **334,** 968–971 (2011).
28. Winkler, C. R., Damodaran, A. R., Karthik, J., Martin, L. W. & Taheri, M. L. Direct observation of ferroelectric domain switching in varying electric field regimes using *in situ* TEM. *Micron* **43,** 1121–1126 (2012).
29. Chang, H. J. *et al.* Watching domains grow: In-situ studies of polarization switching by combined scanning probe and scanning transmission electron microscopy. *J. Appl. Phys.* **110,** 052014 (2011).
30. Phillpot, S. R., Sinnott, S. B. & Asthagiri, A. Atomic-level simulation of ferroelectricity in oxides: Current status and opportunities. *Annu. Rev. Mater. Res.* **37,** 239–270 (2007).
31. Sepliarsky, M., Phillpot, S. R., Wolf, D., Stachiotti, M. G. & Migoni, R. L. Atomic-level simulation of ferroelectricity in perovskite solid solutions. *Appl. Phys. Lett.* **76,** 3986–3988 (2000).
32. Liu, S., Grinberg, I., Takenaka, H. & Rappe, A. M. Reinterpretation of bond-valence model with bond-order formalism: An improved bond-valence-based interatomic potential for $PbTiO_3$. *Phys. Rev. B* **88,** 104102 (2013).
33. Liu, S., Grinberg, I. & Rappe, A. M. Development of a bond-valence based interatomic potential for $BiFeO_3$ for accurate molecular dynamics simulations. *J. Phys. Condens. Matter.* **25,** 102202 (2013).
34. Sepliarsky, M., Stachiotti, M. G. & Migoni, R. L. Surface reconstruction and ferroelectricity in $PbTiO_3$ thin films. *Phys. Rev. B* **72,** 014110 (2005).
35. Takenaka, H., Grinberg, I. & Rappe, A. M. Anisotropic local correlations and dynamics in a relaxor ferroelectric. *Phys. Rev. Lett.* **110,** 147602 (2013).
36. Shin, Y. H., Grinberg, I., Chen, I. W. & Rappe, A. M. Nucleation and growth mechanism of ferroelectric domain-wall motion. *Nature* **449,** 881–887 (2007).
37. Roytburd, A. L. Equilibrium structure of epitaxial layers. *Phys. Status Solidi A* **37,** 329–339 (1976).
38. Ouyang, J. *et al.* Engineering of self-assembled domain architectures with ultra-high piezoelectric response in epitaxial ferroelectric films. *Adv. Funct. Mater.* **17,** 2094–2100 (2007).
39. Romanov, A. E., Vojta, A., Pompe, W., Lefevre, M. J. & Speck, J. S. Domain patterns in (111) oriented tetragonal ferroelectric films. *Phys. Status Solidi A* **172,** 225–253 (1999).
40. Karthik, J., Damodaran, A. R. & Martin, L. W. Epitaxial ferroelectric heterostructures fabricated by selective area epitaxy of $SrRuO_3$ using an MgO mask. *Adv. Mater.* **24,** 1610–1615 (2012).
41. Bassiri-Gharb, N. *et al.* Domain wall contributions to the properties of piezoelectric thin films. *J. Electroceram.* **19,** 47–65 (2007).
42. Sluka, T., Tagantsev, A. K., Dmajanovic, D., Gureev, M. & Setter, N. Enhanced electromechanical response of ferroelectrics due to charged domain walls. *Nature Commun.* **3,** 748 (2012).
43. Kamel, T. M. & de With, G. Double peak switching current in soft ferroelectric lead zirconate titanate. *J. Appl. Phys.* **102,** 044118 (2007).
44. Yin, J. & Cao, W. Polarization reversal study using ultrasound. *Appl. Phys. Lett.* **79,** 4556–4558 (2001).
45. Daniels, J. E. *et al.* Neutron diffraction study of the polarization reversal mechanism in $[111]_C$-oriented $Pb(Zn_{1/3}Nb_{2/3})O_{3-x}PbTiO_3$. *J. Appl. Phys.* **101,** 104108 (2007).
46. Pramanick, A., Prewitt, A. D., Forrester, J. S. & Jones, J. L. Domains, domain walls and defects in perovskite ferroelectric oxides: A review of present understanding and recent contributions. *Crit. Rev. Solid State Mater. Sci.* **37,** 243–275 (2012).
47. Nagarajan, V. *et al.* Dynamics of ferroelastic domains in ferroelectric thin films. *Nature Mater.* **2,** 43–47 (2003).
48. Anbusathaiah, V. *et al.* Labile ferroelastic nanodomains in bilayered ferroelectric thin films. *Adv. Mater.* **21,** 3497–3502 (2009).
49. Meyer, B. & Vanderbilt, D. *Ab initio* study of ferroelectric domain walls in $PbTiO_3$. *Phys. Rev. B* **65,** 104111 (2002).
50. Gao, P. *et al.* Atomic-scale mechanisms of ferroelastic domain-wall-mediated ferroelectric switching. *Nature Commun.* **4,** 2791 (2013).

Acknowledgements

R.X. and S.L. acknowledge support from the National Science Foundation and the Nanoelectronics Research Initiative under grant DMR-1124696. I.G. acknowledges support from the US DOE under grant DE-FG02-07ER46431. J.K. acknowledges support from the National Science Foundation under grant DMR-1451219. A.R.D. and L.W.M. acknowledge support from the Army Research Office under grant W911NF-14-1-0104. A.M.R. acknowledges support from the Office of Naval Research under grant N00014-12-1-1033. The authors acknowledge computational support from the High-Performance Computing Modernization Office of the Department of Defense, and from the National Energy Research Scientific Computing Center of the Department of Energy.

Author contributions

R.X. and L.W.M. designed the experiments. S.L., I.G. and A.M.R. designed the simulation strategy. R.X. performed the experiments. S.L. carried out the MD simulations. R.X., J.K., A.R.D. and L.W.M. analysed the experimental results. S.L., I.G. and A.M.R. analysed the simulation results. R.X., S.L., I.G., A.M.R. and L.W.M. co-wrote the paper.

Additional information

Supplementary information is available in the online version of the paper. Reprints and permissions information is available online at www.nature.com/reprints. Correspondence and requests for materials should be addressed to L.W.M.

Competing financial interests

The authors declare no competing financial interests.